ACS APPLIED MATERIALS & INTERFACES

Research Article

www.acsami.org

Polyphosphoester-Based Nanoparticles with Viscous Flow Core Enhanced Therapeutic Efficacy by Improved Intracellular Drug Release

Yin-Chu Ma, Jun-Xia Wang, Wei Tao, Hai-Sheng Qian, and Xian-Zhu Yang*

School of Medical Engineering, Hefei University of Technology, Hefei, Anhui 230009, People's Republic of China

Supporting Information

ABSTRACT: The intracellular drug release rate from the hydrophobic core of self-assembled nanoparticles can significantly affect the therapeutic efficacy. Currently, the hydrophobic core of many polymeric nanoparticles which are usually composed of poly(ε-caprolactone) (PCL), polylactide (PLA), or poly(D, L-lactide-co-glycolide) (PLGA) may hinder the diffusion of drug from the core because of their glassy state at room temperature. To investigate the effect of the hydrophobic core state on therapeutic efficacy, we synthesized an amphiphilic diblock copolymers of hydrophilic poly(ethylene glycol) (PEG) and hydrophobic polyphosphoester, which were in a viscous flow state at room temperature. The obtained copolymers self-assembled into core−shell nanoparticles, which efficiently encapsulate doxorubicin (DOX) in the hydrophobic polyphosphoester core (NP_{PPE}/DOX). As speculated, compared with the nanoparticles bearing glassy core (hydrophobic PLA core, NP_{PLA}/DOX), the encapsulated DOX was more rapidly released from NP_{PPE}/DOX with viscous flow core, resulting in significantly increased cytotoxicity. Accordingly, the improved intracellular drug release from viscous flow core enhances the inhibition of tumor growth, suggesting the nanoparticles bearing viscous flow core show great potential in cancer therapy.

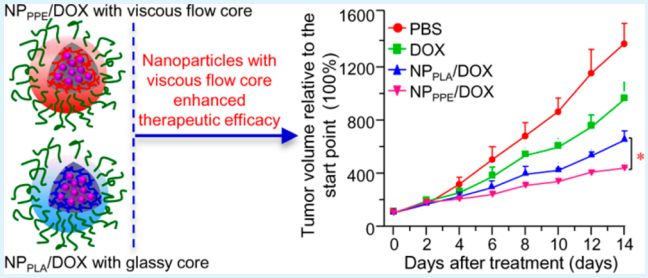

KEYWORDS: *hydrophobic polyphosphoester, intracellular drug release, drug delivery, cancer therapy, delivery systems*

INTRODUCTION

Cancer has become one of the main causes of death in the world, and chemotherapy remains as one of the main treatments along with surgery.[1] However, the therapeutic efficacy of traditional chemotherapeutic drug is far from satisfactory, and it is urgently desired to improve therapeutic efficacy of chemotherapy.[2,3] In the past few decades, nanoscale delivery systems for cancer therapy have attracted much attention due to the improved pharmacokinetics and biodistribution profile via enhanced permeability and retention (EPR) effect.[4−6] Up to this point, nearly 250 nanoparticles-based drug or drug candidates have been under clinical trials at different stages or preclinical development.[7] Some, such as Doxil, Genexol-PM, and Abraxane, have been approved for clinical applications.[8] Doxil, a PEG-liposomal formulation of doxorubicin, was first approved, and Genexol-PM, a paclitaxel-loaded self-assembled polymeric nanoparticles, was the first approved polymeric nanoparticles-based drugs for breast cancer treatment. In spite of these successes, the therapeutic efficacies of these nanoscale drug delivery systems still suffer from limitations. For example, although the enhanced drug accumulation in solid tumor was found via the delivery of Doxil compared to the free doxorubicin, the antitumor efficacy is still affected by the poor release from the nanoparticles.[9] Therefore, after accumulation in tumor site and uptake by tumor cells, the intracellular drug release rate from the nanoparticles plays an important role in the therapeutic efficacy and can be improved upon.[10−14]

Self-assembled nanoparticles, which were composed of amphiphilic block copolymers, can efficiently encapsulate hydrophobic anticancer drugs into the hydrophobic core.[15−17] As demonstrated in the phase 1 clinical data of BIND-014 (docetaxel loaded mPEG−PLA based nanoparticles), the release rate of loaded drug depended on the composition of the hydrophobic core of the nanoparticles.[18] Among the current polymeric drug delivery system, the hydrophobic core is usually composed of PLA, PLGA, or PCL.[19] These commonly used materials are in the glassy state at room temperature. Thus, the molecular motions of the polymeric core are mainly restrained to vibrations and short-range rotational motions,[20] which may affect the diffusion of drug from nanoparticles and subsequent anticancer efficacy. In contrast, polyphosphoesters (PPEs) are in a viscous flow state at room temperature.[21−26] Therefore, the molecular motions are significantly increased compared to the commonly used materials, which may improve the drug release from the PPE based core. PPEs are used as

Received: June 30, 2014
Accepted: September 4, 2014
Published: September 4, 2014

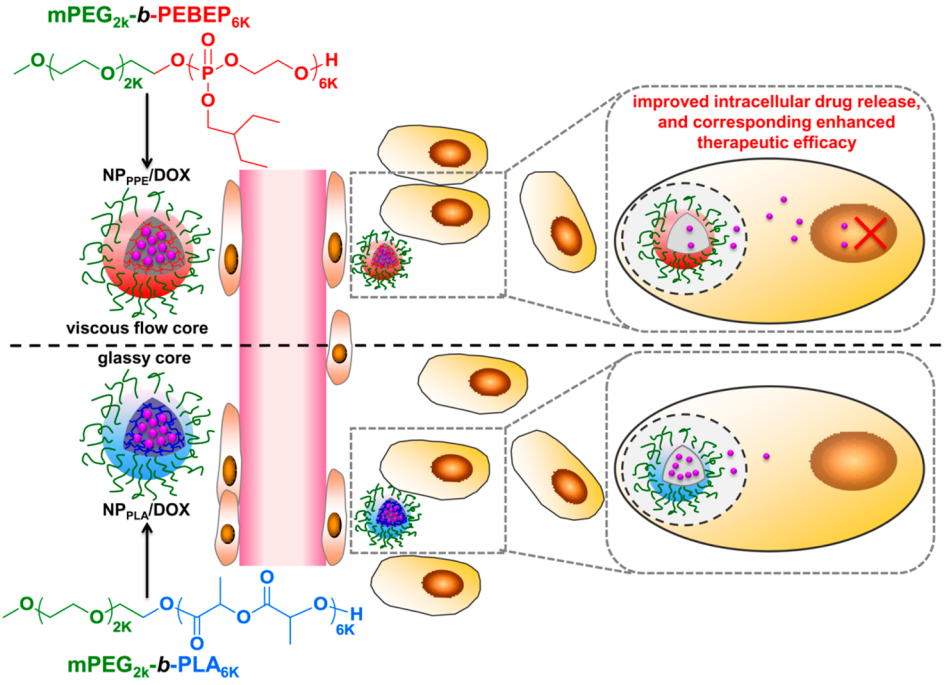

Figure 1. Schematic illustration of the effect of the hydrophobic core state on therapeutic efficacy of drug-loaded nanoparticles. NP_{PPE}/DOX: $mPEG_{2k}$-*b*-$PEBEP_{6k}$ (diblock polymer of mPEG and PPE, the subscript number represents molecular weight of each block) based nanoparticles encapsulated DOX in the hydrophobic PPE core; NP_{PLA}/DOX: $mPEG_{2k}$-*b*-PLA_{6k} (diblock polymer of mPEG and PLA, the subscript number represents molecular weight of each block) based nanoparticles encapsulated DOX in the hydrophobic PLA core.

hydrophilic polymer for biomedical applications.[24,27,28] Up to now, only thermosensitive PPEs, namely, poly(ethyl ethylene phosphate) with high molecular weights becomes hydrophobic above lower critical solution temperature (LCST), which allows them to be used as hydrophobic core of drug delivery systems.[29] In addition, Both Wang's and Wooley's groups have conjugated the hydrophobic anticancer drugs to the poly(ethylene glycol)-*block*-polyphosphoester. The obtained polymer could then form nanoparticles due to the hydrophobicity of the drugs.[30,31] However, the therapeutic efficacy of drug loaded self-assembled nanoparticles, which were prepared by block copolymers of hydrophobic PPE and hydrophilic PEG, were rarely reported.

To demonstrate the effect of the state of the hydrophobic core on therapeutic efficacy, we first synthesized amphiphilic block copolymers of PEG and PPE, which can self-assemble into core−shell nanoparticles bearing a viscous flow hydrophobic PPE core. The hydrophobic PPE core allows the hydrophobic DOX (NP_{PPE}/DOX) encapsulation (Figure 1), and the PEG-*b*-PLA based nanoparticles (NP_{PLA}/DOX) bearing glassy core were used as a control. With the presence of PEG layer, both nanoparticles exhibited excellent serum stability and efficient delivery comparable to DOX into MDA-MB-231 breast cancer cells. In addition, we demonstrated the biodistribution and pharmacokinetics of both nanoparticles were also similar after systemic administration. However, DOX release from viscous flow core of NP_{PPE}/DOX was significantly faster than that from the glassy core, which significantly increased cytotoxicity to tumor cells. Accordingly, this improved intracellular DOX release further enhances the tumor-growth-suppression efficiencies.

EXPERIMENTAL SECTION

Materials and Characterizations. 3-(4,5-Dimethylthiazol-2-yl)-2,5-diphenyl tetrazolium bromide (MTT) were purchased from Sigma-Aldrich. Ultrapurified water was obtained using a Milli-Q Synthesis System (Millipore, Bedford, MA, USA). Doxorubicin hydrochloride (DOX·HCl) was purchased from Zhejiang Hisun Pharmaceutical Co., Ltd. (China). Dulbecco's modified Eagle's medium (DMEM) and L-glutamine were purchased from Gibco BRL (Eggenstein, Germany). The diblock copolymer $mPEG_{2K}$-*b*-PLA_{6K} was synthesized according to a previously reported method.[32] Other organic solvents or reagents were used as received.

The size of the nanoparticles was measured according to a previously reported method.[25] The morphology of nanoparticles was analyzed by JEOL-2010 transmission electron microscopy (TEM) at an accelerating voltage of 200 kV. The concentration of doxorubicin (DOX) was determined by high-performance liquid chromatography (HPLC) according to previously reported method.[33,34]

Preparation of DOX-Loaded Nanoparticles. The dialysis method was used to prepare DOX-loaded nanoparticles. Before loading DOX, DOX·HCl (1.0 mg, 1.72 μmol) was stirred overnight with triethylamine (0.35 mg, 3.44 μmol) in dimethyl sulfoxide (DMSO, 1.0 mL) to obtain the DOX base. Then, the polymer $mPEG_{2k}$-*b*-$PEBEP_{6K}$ (10.0 mg) was added dropwise, and the solution was stirred for another 3 h. The final solution was transferred to a dialysis tube (MWCO 3500), and dialyzed against ultrapure water for 24 h. Furthermore, unloaded DOX was removed through a 0.45 μm filter (Millipore), and the obtained DOX-loaded nanoparticels was denoted as NP_{PPE}/DOX. The control DOX-loaded nanoparticles (NP_{PLA}/DOX) were prepared using a similar method as descripted above, except that $mPEG_{2K}$-*b*-PLA_{6K} was used to replace the $mPEG_{2k}$-*b*-$PEBEP_{6K}$. To determine drug loading content (DLC) and encapsulation efficiencies (EE), the DOX-loaded nanoparticles solution was lyophilized. Then, the lyophilized nanoparticles were weighted and redissolved in DMSO. The DOX concentration was determined according to previous method using HPLC analyses.[33,34] The DLC and EE were calculated by the following equations:

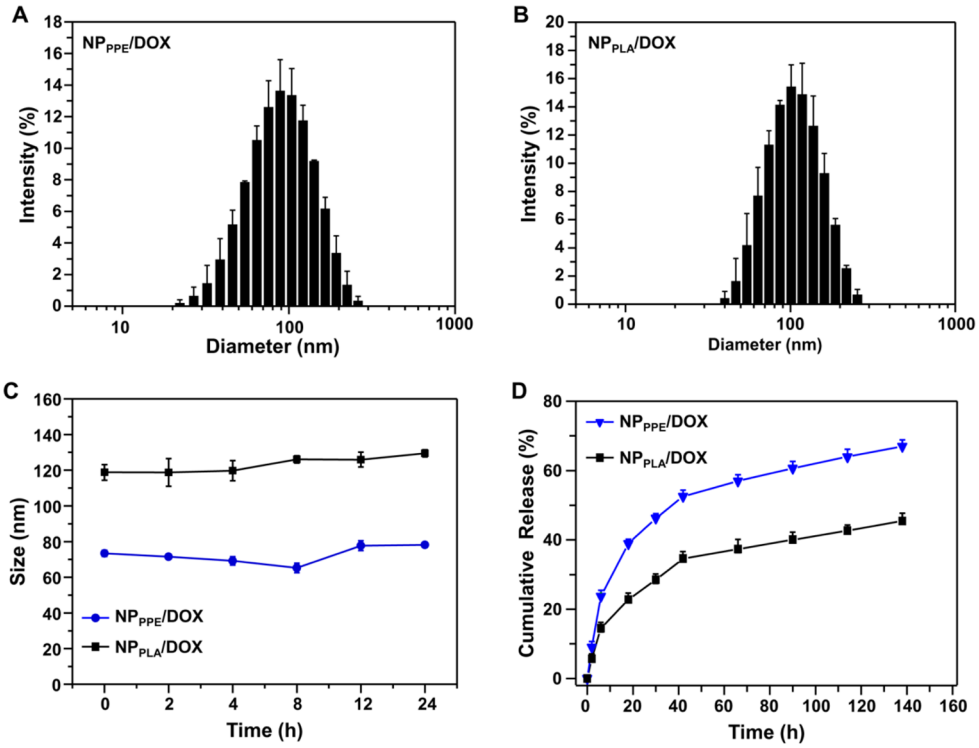

Figure 2. (A, B) Intensity distribution of particle size of DOX loaded nanoparticles (NP_{PPE}/DOX and NP_{PLA}/DOX). (C) Changes in size of the nanoparticles NP_{PPE}/DOX and NP_{PLA}/DOX after incubation with 10% FBS in DMEM medium. (D) In vitro DOX release from NP_{PPE}/DOX and NP_{PLA}/DOX.

$$\text{DLC}\ (\%) = \frac{\text{amount of DOX in nanoparticles}}{\text{amount of DOX} - \text{loaded nanoparticles}} \times 100\%$$

$$\text{EE}(\%) = \frac{\text{amount of DOX in nanoparticles}}{\text{amount of DOX added}} \times 100\%$$

In Vitro Release of DOX from Nanoparticles. NP_{PPE}/DOX and NP_{PLA}/DOX were suspended in phosphate buffer (PB, 0.02 M, pH 7.4) at 1.0 mg mL^{-1} in the dialysis membrane tubing (MW cutoff = 14 000), and the tubing was immersed in 10 mL of PB at 37 °C in a shaking water bath. At predetermined time points, the external buffer was collected, and the fresh PB with equal volume was added. The collected solution was freeze-dried and redissolved in the mixture solution of acetonitrile/water (50/50, v/v) to determine the concentration of doxorubicin.[33,34]

Cell Culture. The human breast cancer cell line MDA-MB-231 from the American Type Culture Collection (ATCC) were used to evaluate both nanoparticles, this cells were cultured as previously reported method.[31]

Cytotoxicity Measurement. The cytotoxicity of blank nanoparticles prepared by $mPEG_{2k}$-*b*-$PEBEP_{6k}$ or $mPEG_{2k}$-*b*-PLA_{6k} was assessed with a MTT viability assay against MDA-MB-231 cells. Such protocol has been descripted in our previously method.[35]

Cellular Uptake of Nanoparticles and Intracellular Trafficking. To analyze cellular uptake of nanoparticles, MDA-MB-231 cells (5.0×10^4 cells per well) were seeded onto 24-well plates. After it was cultured at 37 °C for 24 h, the medium was replaced with fresh medium containing free DOX, NP_{PPE}/DOX and NP_{PLA}/DOX. The final concentration of DOX in the culture medium was 4.0 μg/mL. After incubating with different formulations for 2 or 4 h, the cells were rinsed and the subsequent protocol has been described previously.[35]

To analyze the intracellular distribution of DOX with the delivery of nanoparticles, the MDA-MB-231 cells were seeded on coverslips on a 24-well plate at 1×10^5 cells per well and further incubated for 24 h. The original medium was removed, and fresh medium containing NP_{PPE}/DOX or NP_{PLA}/DOX were added as described above. At different time points, the cells were washed twice with cold PBS, and the subsequent protocol has been described previously.[36]

In Vitro Cytotoxicity Assays. Cytotoxicities of free DOX, NP_{PPE}/DOX, and NP_{PLA}/DOX were evaluated by MTT viability assay. The MDA-MB-231 cells were seeded onto 96-well plates at 2.0×10^3 cells per well and further incubated for 24 h. The cells were incubated with the different formulations at different DOX concentrations for 48 h. The cell viability was determined as described above, and the 50% cellular growth inhibition (IC_{50}) values were determined from the MTT assay.

Plasma Pharmacokinetics. Sixty-three BALB/c mice were randomly divided into three groups. Free DOX, NP_{PPE}/DOX, and NP_{PLA}/DOX were intravenously injected at a DOX dose of 10.0 mg/kg. At the predetermined time point, the blood samples (three mice for each group) were collected, and then the plasma DOX concentration was analyzed by HPLC according to previously reported methods.[31]

Animal Models. BALB/c nude mice (6 weeks old) were purchased from the Shanghai Experimental Animal Centre of the Chinese Academy of Sciences (Shanghai, China) and all animals received care in compliance with the guidelines outlined in the *Guide for the Care and Use of Laboratory Animals*. The xenograft tumor model was generated as described previously.[31]

Tissue Biodistribution. Free DOX, NP_{PPE}/DOX, and NP_{PLA}/DOX were administrated intravenously into mice bearing MDA-MB-231 tumors. The injection dose of DOX was 10.0 mg of DOX per kg of mouse body weight. At the predetermined time point, these mice were sacrificed, and then the solid tumor tissues and main organs were harvested and imaged by a Xenogen IVIS Lumina system (Caliper Life Sciences, U.S.A.). Then, the organs were homogenized for quantitative assay.[31]

Tumor Suppression Study. The MDA-MB-231 tumor-bearing mice were randomly divided into four groups (five mice per group). These mice were treated with free DOX, NP_{PPE}/DOX, NP_{PLA}/DOX, or PBS by intravenous injection once every other day. The dose of DOX was 5.0 mg kg^{-1} per injection. The estimated tumor volume was calculated according to the following formula: tumor volume (mm^3) =

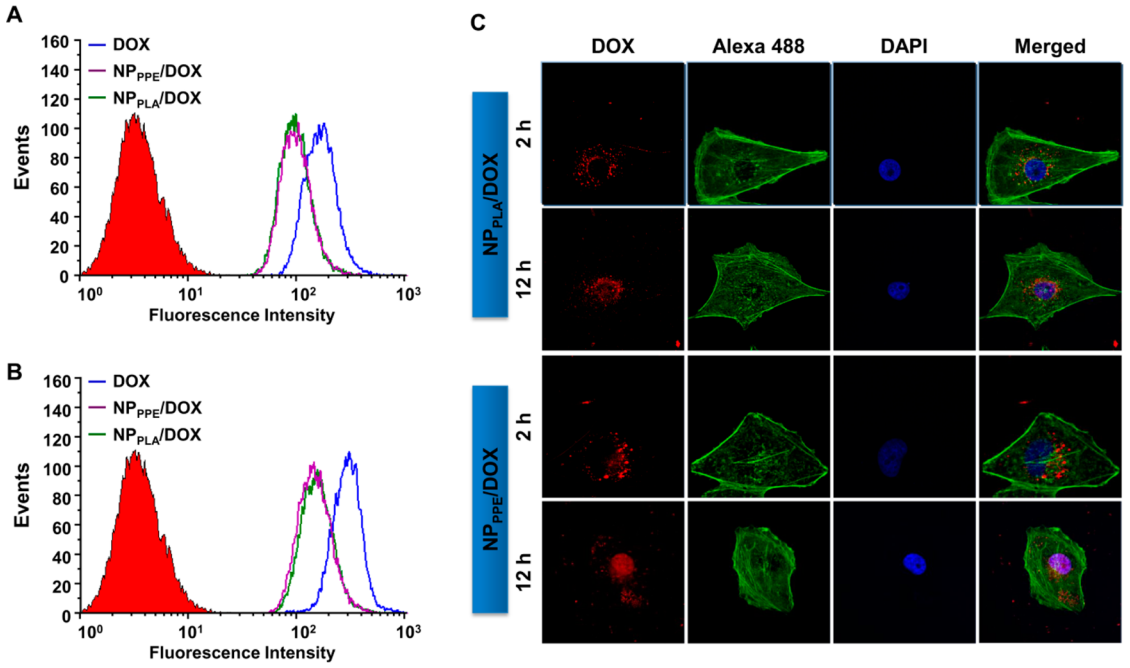

Figure 3. (A, B) Flow cytometric analyses of cellular internalization of NP_{PPE}/DOX and NP_{PLA}/DOX in MDA-MB-231 cells after incubation for 2 h (A) or 4 h (B), respectively. (C) CLSM images of cell distribution of NP_{PPE}/DOX or NP_{PLA}/DOX after incubation for 2 or 12 h with MDA-MB-231 cells. Cell cytoskeleton F-actin was stained with Alexa Fluor 488 phalloidin, and cell nuclei was stained with and DAPI. The final concentration of DOX in the culture medium was 4.0 μg/mL.

0.5 × length × width^2. The length and width were monitored using calipers.

Immunohistochemical Analysis. One day after the last injection, the mice were sacrificed and tumor tissues were excised, fixed in 4% formaldehyde and embedded in paraffin. Then, paraffin-embedded 5 μm tumor sections were obtained. Cell proliferation and apoptosis in tumor tissue were also analyzed by immunnohistochemical staining of the proliferating cell nuclear antigen (PCNA) and the terminal transferase dUTP nick-end labeling (TUNEL) assay.[35]

Statistical analysis. To measure statistical differences among groups, statistical analyses were performed using Student's *t test*. Data with $p < 0.05$ were considered to be statistically significant.

RESULTS AND DISCUSSION

Preparation and Characterization of DOX-Loaded Nanoparticles NP_{PPE}/DOX and NP_{PLA}/DOX. To obtain nanoparticles with a viscous flow hydrophobic core, we synthesized mPEG-*b*-PEBEP diblock copolymers by 1,5,7-Triazabicylo[4.4.0]dec-5-ene (TBD) catalyzed ring-opening polymerization of hydrophobic cyclic phosphate monomers EBEP. Successful synthesis of $mPEG_{2k}$-*b*-$PEBEP_{6K}$ was confirmed by GPC analyses (Supporting Information Figure S1A) and NMR (Supporting Information Figure S1B). $mPEG_{2k}$-*b*-PLA_{6K} was prepared as a control. Thermal properties of $mPEG_{2k}$-*b*-$PEBEP_{6K}$ and $mPEG_{2k}$-*b*-PLA_{6K} were investigated by differential scanning calorimetry (DSC). As shown in Supporting Information Figure S2, the glass transition temperature (T_g) for $mPEG_{2k}$-*b*-$PEBEP_{6K}$ was about −57 °C, which is the result of its highly viscous liquid form at room temperature. Similar results have been reported by other groups.[26,37] In addition, melting temperature (T_m) for the PEG block segment of both diblock copolymers was lower than that of the $mPEG_{2k}$−OH, which may be because that PLA blocks or PPE block affects the crystallization of PEG.[38]

To demonstrate the self-assembly of the obtained $mPEG_{2k}$-*b*-$PEBEP_{6K}$ and $mPEG_{2k}$-*b*-PLA_{6K}, the excitation spectra of pyrene was measured with increased concentration of both polymers. As shown in Supporting Information Figure S3A, when the concentration of $mPEG_{2k}$-*b*-$PEBEP_{6K}$ increased, a red shift of the fluorescence excitation spectra of pyrene has been found, which indicated the formation of aggregation. Supporting Information Figure S3B shows the critical aggregation concentrations of $mPEG_{2k}$-*b*-$PEBEP_{6K}$ and $mPEG_{2k}$-*b*-PLA_{6K} polymer were 0.96 and 3.61 mg/L, respectively.

In this study, DOX was used as a model anticancer drug to evaluate the efficiency of the both delivery system with different core states. DOX was loaded into polymeric nanoparticles by the dialysis method. The encapsulation efficiencies of $mPEG_{2k}$-*b*-$PEBEP_{6K}$ and $mPEG_{2k}$-*b*-PLA_{6K} were 48.5% ± 2.3% and 56.7% ± 1.9%, respectively. After DOX loading, as shown in Figure 2A and Figure 2B, the average size of NP_{PPE}/DOX was similar to that of NP_{PLA}/DOX, and both DOX-loaded nanoparticles were slight larger than the corresponding blank nanoparticles (Supporting Information Figure S3C and S3D). For structural characterization, both DOX loaded nanoparticles were imaged by TEM (Supporting Information Figure S4), showing a compact and spherical morphology.

The stability of drug-loaded delivery system is closely correlated to its destiny in vivo. Therefore, we incubated the DOX-loaded nanoparticles NP_{PPE}/DOX and NP_{PLA}/DOX in culture medium containing 10% FBS to study their stability at 37 °C. At different time intervals, the size of these nanoparticles was measured. As shown in Figure 2C, the size was maintained for about 2 days for both nanoparticles, which may be due to the PEG shell presented at the surface of nanoparticles was capable of preventing aggregation of nanoparticles.

To investigate the effect of the hydrophobic core state on the drug release rate, the in vitro release profile of DOX from nanoparticles bearing different core was taken. As shown in Figure 2D, the cumulative DOX release from NP_{PPE}/DOX

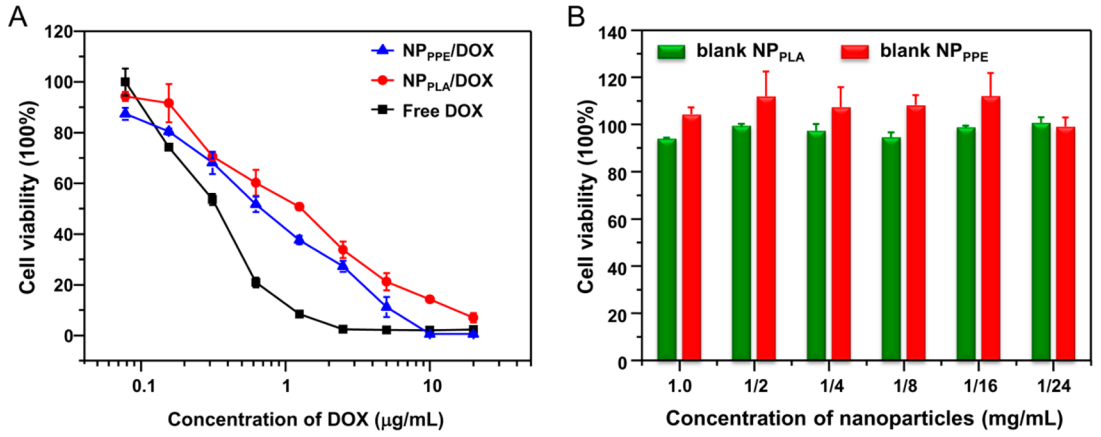

Figure 4. (A) MTT viability assay was used to determine the cell viability of MDA-MB-231 cells after incubation with NP$_{PPE}$/DOX, NP$_{PLA}$/DOX, or free DOX. (B) Cytotoxicity of blank nanoparticles without DOX encapsulation to MDA-MB-231 cells.

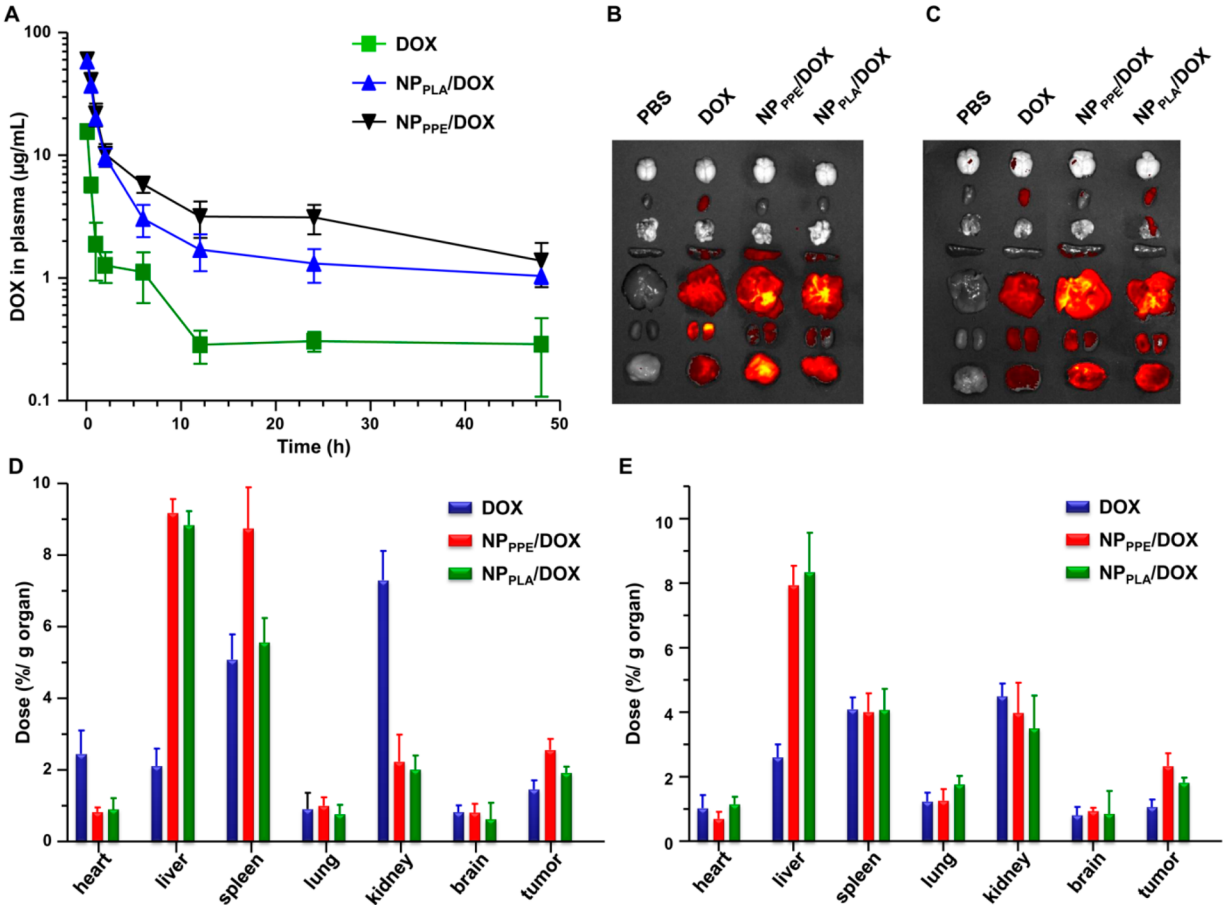

Figure 5. (A) Plasma DOX concentration versus time following administration of NP$_{PPE}$/DOX, NP$_{PLA}$/DOX or free DOX (mean ± SD, n = 3). (B, C) Fluorescence images of main organs after administration of NP$_{PPE}$/DOX, NP$_{PLA}$/DOX, PBS or free DOX at 6 h (B) and 12 h (C). (D, E) Quantitative analyses of DOX distribution in main organs at 6 h (D) and 24 h (E) after administration of different formulations (mean ± SD, n = 3).

bearing viscous flow core were approximately 40% after 20 h of incubation. In contast, only 23% of the loaded DOX were released from nanoparticles NP$_{PLA}$/DOX with glassy core. We had speculated that the DOX release from nanoparticles with viscous flow core was significantly faster than that from glassy core. However, it should be noted that the drug release rate may also be affected by the degradation rate of the polymeric carriers. Therefore, the degradation of both blank nanoparticles was detected. As shown in Supporting Information Figure S5, both polymers were almost not degraded within 144 h (the last time point of the drug release), which confirmed the above speculation.

Cellular Internalization and Intracellular Drug Release Behaviors of NP$_{PPE}$/DOX and NP$_{PLA}$/DOX. The cellular internalization of NP$_{PPE}$/DOX and NP$_{PLA}$/DOX was evaluated by the intracellular fluorescence using flow cytometry after incubation with both nanoparticles at 37 °C for 2 and 4 h. As shown in Figure 3A and 3B, following incubation with either

dx.doi.org/10.1021/am5042466 | ACS Appl. Mater. Interfaces 2014, 6, 16174−16181

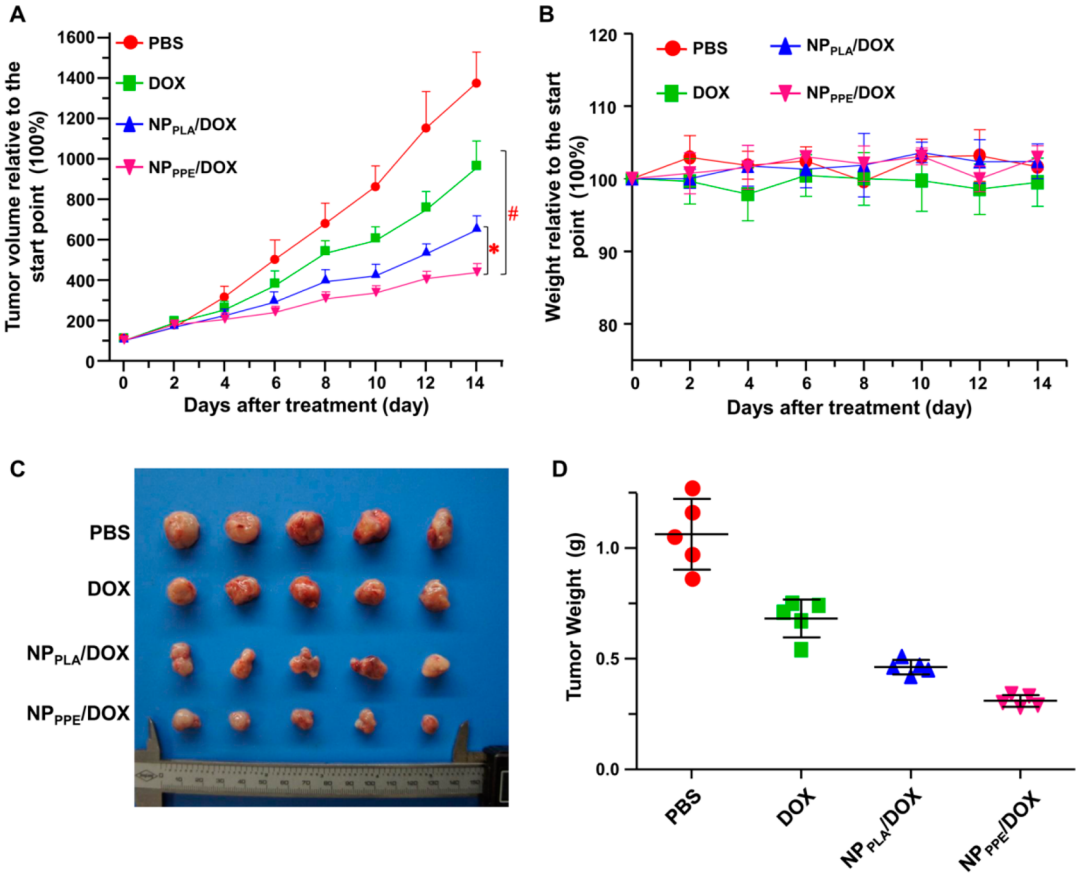

Figure 6. (A) Antitumor effect in MDA-MB-231 breast cancer xenografts after treatment with different formulations (n = 6). $^{*}p < 0.05$ when compared with NP$_{PLA}$/DOX; $^{\#}p < 0.01$ when compared with DOX. (B) Body weight of mice bearing MDA-MB-231 breast cancer xenografts at different time points after treatment with above formulations. (C, D) Images (C) and Weights (D) of MDA-MB-231 xenograft tumors at the final time point of the treatment.

NP$_{PPE}$/DOX or NP$_{PLA}$/DOX, there is no significant difference in the MDA-MB-231 cells. This indicates that the state of the core of nanoparticles did not affect the cellular uptake of DOX. Moreover, it is noteworthy that the cells incubated with free DOX alone exhibited stronger intracellular fluorescence. This is because the fluorescence of DOX was quenched after encapsulation into nanoparticles (data not shown).

The intracellular DOX release behaviors of both NP$_{PPE}$/DOX and NP$_{PLA}$/DOX were further analyzed by CLSM observations. The cells were treated with either NP$_{PPE}$/DOX or NP$_{PLA}$/DOX for different periods of time, and the localization of NP$_{PPE}$/DOX and NP$_{PLA}$/DOX was further observed. As shown in Figure 3C, both NP$_{PPE}$/DOX and NP$_{PLA}$/DOX were mainly localized in the cytoplasm after 2 h of incubation. However, it could be found that cells cultured with NP$_{PPE}$/DOX had much stronger intracellular red fluorescent signals in the cell nuclei at 12 h than cells treated with NP$_{PLA}$/DOX. This result could be because the DOX release from a viscous flow core was significantly faster than that from a glassy core. This resulted in more DOX accumulated in nuclei.

In Vitro Cytotoxicity Assay of NP$_{PPE}$/DOX and NP$_{PLA}$/DOX. As reported, DOX interacted with the major groove area of DNA in the cell nucleus, which inhibited the replication, transcription, and translation of DNA and caused cell death. Therefore, the enhanced DOX accumulated in nuclei by NP$_{PPE}$/DOX may be accompanied by increased cytotoxicity to tumor cells. To demonstrate this, the cancer cells were incubated with NP$_{PPE}$/DOX or NP$_{PLA}$/DOX for 48 h. MTT viability assay was used to determine the cell proliferation. As shown in Figure 4A, the growth of the cells was inhibited in a dose-dependent manner for both NP$_{PPE}$/DOX and NP$_{PLA}$/DOX. However, NP$_{PPE}$/DOX was more effectively inhibited tumor cell growth than the NP$_{PLA}$/DOX, and the IC$_{50}$ value of the NP$_{PPE}$/DOX treatment in tumor cells was 0.67 μg/mL, which was ca. 2-fold lower than that of treatment with NP$_{PLA}$/DOX (IC$_{50}$ = 1.31 μg/mL). Moreover, both blank NP$_{PPE}$ (prepared by mPEG$_{2k}$-b-PEBEP$_{6k}$) and NP$_{PLA}$ (prepared by mPEG$_{2k}$-b-LA$_{6k}$), even at the higher concentration did not exhibit cytotoxicity to the cancer cells (Figure 4B). This result demonstrated that the inhibition of cell proliferation was not caused because of the cytotoxicity of the blank nanoparticles. These results indicated that drug-loaded nanoparticles with viscous flow cores exhibited improved cytotoxicity to tumor cells when compared to those bearing glassy cores.

Plasma Pharmacokinetics and Biodistribution. To investigate the effect of the state of the core on in vivo pharmacokinetics and biodistribution, both NP$_{PPE}$/DOX, NP$_{PLA}$/DOX, and free DOX were intravenously injected into mice. The blood was collected, and the plasma DOX concentration was determined by HPLC. As shown in Figure 5A, DOX delivered by NP$_{PPE}$/DOX or NP$_{PLA}$/DOX showed a prolonged half-life in blood circulation, compared with free DOX. Meanwhile, the NP$_{PPE}$/DOX and NP$_{PLA}$/DOX significantly increased the area under the curve (AUC) in blood in contrast to the free DOX.

In addition, the biodistributions of NP_{PPE}/DOX, NP_{PLA}/DOX, and free DOX were imaged (Figure 5B and 5C). The free DOX showed the weakest fluorescence, because it was rapidly cleared from the circulation as described above. Moreover, the fluorescence in the tumor tissue with the intravenous injection of NP_{PPE}/DOX was much stronger than NP_{PLA}/DOX at both times. However, the quantitative data of DOX (Figure 5D and 5E) showed that DOX accumulation in tumors tissue after administration of NP_{PPE}/DOX was slightly higher at both time interval than that administration of NP_{PLA}/DOX, which may be resulted from the faster DOX release rate from the viscous flow core of NP_{PPE}/DOX as demonstrated in Figure 2D.

In Vivo Antitumor Efficacy. The enhanced drug release rate of DOX from the viscous flow core of NP_{PPE}/DOX could potentially enhance the antitumor efficacy. To demonstrate this, the antitumor effect was examined by one intravenous injection of NP_{PPE}/DOX and NP_{PLA}/DOX every other day in mice with MDA-MB-231 xenografts. The injection dose of DOX dose was 5.0 mg kg^{-1} per injection. Free DOX was used as controls. As illustrated in Figure 6A, treatment with the NP_{PPE}/DOX showed the best tumor growth inhibition. Moreover, it is worth noting that there was not t significant body weight loss at this DOX doses (Figure 6B). This suggests that the antitumor efficacy resulted from the DOX rather than the cytotoxicity of the nanoparticles. Furthermore, after the last measurement, the tumor mass was excised for imaging and weighting. As expected, following treatment with NP_{PPE}/DOX, the volume of the tumor was minimal, and the weight of the tumor mass was the lowest (Figure 6C and 6D).

Cell apoptosis and proliferation in tumor tissue were also analyzed by immunnohistochemical staining of the TUNEL and the PCNA assay. In Figure 7, the administration of NP_{PPE}/DOX when compared with free DOX or NP_{PLA}/DOX, significantly reduced the PCNA-positive tumor cells and increased TUNEL-positive tumor cells. These above data confirm that the NP_{PPE}/DOX can significantly enhance the antitumor efficacy of DOX by the enhanced drug release from the viscous flow core, indicating that the nanoparticles with viscous flow core has remarkable potential as drug delivery carrier for cancer therapy.

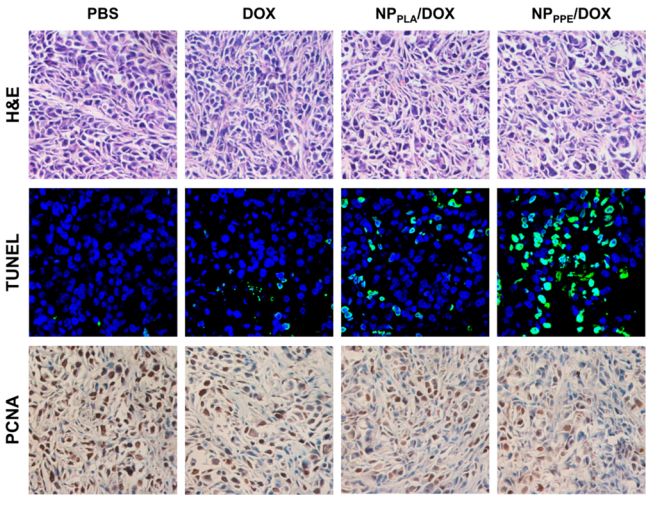

Figure 7. H&E, PCNA, and TUNEL analyses of tumor tissues at the last time point of the treatment. The brown cells represented the PCNA-positive proliferating cells, and the green cells represented the TUNEL-positive apoptotic cells.

CONCLUSIONS

The effect of the state of hydrophobic core on therapeutic efficacy of drug-loaded nanoparticles has rarely been studied. To investigate this, nanoparticles bearing viscous flow PPE core or glassy PLA core were developed. We demonstrated that DOX release from viscous flow core of NP_{PPE}/DOX is significantly faster than that from glassy PLA core, resulting in significantly increased cytotoxicity to tumor cells. More importantly, NP_{PPE}/DOX significantly improved tumor growth inhibition due to the faster intracellular DOX release, indicating that the drug-loaded nanoparticles with viscous flow core show great potential for improved therapeutic therapy of cancer.

ASSOCIATED CONTENT

Supporting Information

The synthesis and characterizations of $mPEG_{2k}$-*b*-$PEBEP_{6K}$ diblock copolymer. This material is available free of charge via the Internet at http://pubs.acs.org.

AUTHOR INFORMATION

Corresponding Author

*E-mail: yangxz@hfut.edu.cn.

Author Contributions

Y. C. Ma and J. X. Wang contributed equally.

Notes

The authors declare no competing financial interest.

ACKNOWLEDGMENTS

This work was supported by the Ministry of Science and Technology of the People's Republic of China (2014AA020708), the National Natural Science Foundation of China (51473043, 51203145, 21304028, 51390482), the Fundamental Research Funds for the Central Universities (2014HGCH0014, 2013HGCH0001).

REFERENCES

(1) Bray, F.; Jemal, A.; Grey, N.; Ferlay, J.; Forman, D. Global Cancer Transitions According to the Human Development Index (2008–2030): A Population-Based Study. *Lancet Oncol.* **2012**, *13*, 790–801.

(2) Peer, D.; Karp, J. M.; Hong, S.; FaroKhzad, O. C.; Margalit, R.; Langer, R. Nanocarriers as an Emerging Platform for Cancer Therapy. *Nat. Nanotechnol.* **2007**, *2*, 751–760.

(3) Wei, H.; Zhuo, R. X.; Zhang, X. Z. Design and Development of Polymeric Micelles with Cleavable Links for Intracellular Drug Delivery. *Prog. Polym. Sci.* **2013**, *38*, 503–535.

(4) Hoffman, A. S. The Origins and Evolution of "Controlled" Drug Delivery Dystems. *J. Controlled Release* **2008**, *132*, 153–163.

(5) Maeda, H.; Wu, J.; Sawa, T.; Matsumura, Y.; Hori, K. Tumor Vascular Permeability and the EPR Effect in Macromolecular Therapeutics: a Review. *J. Controlled Release* **2000**, *65*, 271–284.

(6) Fang, J.; Nakamura, H.; Maeda, H. The EPR Effect: Unique Features of Tumor Blood Vessels for Drug Delivery, Factors Involved, and Limitations and Augmentation of the Effect. *Adv. Drug Delivery Rev.* **2011**, *63*, 136–151.

(7) Kamaly, N.; Xiao, Z.; Valencia, P. M.; Radovic-Moreno, A. F.; Farokhzad, O. C. Targeted Polymeric Therapeutic Nanoparticles: Design, Development and Clinical Translation. *Chem. Soc. Rev.* **2012**, *41*, 2971–3010.

(8) Jain, R. K.; Stylianopoulos, T. Delivering Nanomedicine to Solid Tumors. *Nat. Rev. Clin. Oncol.* **2010**, *7*, 653–664.

(9) Barenholz, Y. Doxil (R)—The First FDA-Approved Nano-Drug: Lessons Learned. *J. Controlled Release* **2012**, *160*, 117−134.
(10) Li, Z. Y.; Liu, Y.; Wang, X. Q.; Liu, L. H.; Hu, J. J.; Luo, G. F.; Chen, W. H.; Rong, L.; Zhang, X. Z. One-Pot Construction of Functional Mesoporous Silica Nanoparticles for the Tumor-Acidity-Activated Synergistic Chemotherapy of Glioblastoma. *ACS Appl. Mater. Interfaces* **2013**, *5*, 7995−8001.
(11) Ge, Z.; Liu, S. Functional Block Copolymer Assemblies Responsive to Tumor and Intracellular Microenvironments for Site-Specific Drug Delivery and Enhanced Imaging Performance. *Chem. Soc. Rev.* **2013**, *42*, 7289−7325.
(12) Bae, Y.; Kataoka, K. Intelligent Polymeric Micelles from Functional Poly(Ethylene Glycol)−Poly(Amino Acid) Block Copolymers. *Adv. Drug Delivery Rev.* **2009**, *61*, 768−784.
(13) Sahoo, B.; Devi, K. S. P.; Banerjee, R.; Maiti, T. K.; Pramanik, P.; Dhara, D. Thermal and pH Responsive Polymer-Tethered Multifunctional Magnetic Nanoparticles for Targeted Delivery of Anticancer Drug. *ACS Appl. Mater. Interfaces* **2013**, *5*, 3884−3893.
(14) Zhao, Y.; Alakhova, D. Y.; Kim, J. O.; Bronich, T. K.; Kabanov, A. V. A Simple Way to Enhance Doxil (R) Therapy: Drug Release from Liposomes at the Tumor Site by Amphiphilic Block Copolymer. *J. Controlled Release* **2013**, *168*, 61−69.
(15) Park, J. H.; Lee, S.; Kim, J. H.; Park, K.; Kim, K.; Kwon, I. C. Polymeric Nanomedicine for Cancer Therapy. *Prog. Polym. Sci.* **2008**, *33*, 113−137.
(16) Zhang, L.; Chan, J. M.; Gu, F. X.; Rhee, J. W.; Wang, A. Z.; Radovic-Moreno, A. F.; Alexis, F.; Langer, R.; Farokhzad, O. C. Self-Assembled Lipid-Polymer Hybrid Nanoparticles: a Robust Drug Delivery Platform. *ACS Nano* **2008**, *2*, 1696−1702.
(17) Wiradharma, N.; Zhang, Y.; Venkataraman, S.; Hedrick, J. L.; Yang, Y. Y. Self-Assembled Polymer Nanostructures for Delivery of Anticancer Therapeutics. *Nano Today* **2009**, *4*, 302−317.
(18) Hrkach, J.; Von Hoff, D.; Ali, M. M.; Andrianova, E.; Auer, J.; Campbell, T.; De Witt, D.; Figa, M.; Figueiredo, M.; Horhota, A.; Low, S.; McDonnell, K.; Peeke, E.; Retnarajan, B.; Sabnis, A.; Schnipper, E.; Song, J. J.; Song, Y. H.; Summa, J.; Tompsett, D.; Troiano, G.; Hoven, T. V. G.; Wright, J.; LoRusso, P.; Kantoff, P. W.; Bander, N. H.; Sweeney, C.; Farokhzad, O. C.; Langer, R.; Zale, S. Preclinical Development and Clinical Translation of a PSMA-Targeted Docetaxel Nanoparticle with a Differentiated Pharmacological Profile. *Sci. Transl. Med.* **2012**, *4*, 128ra39.
(19) Soppimath, K. S.; Aminabhavi, T. M.; Kulkarni, A. R.; Rudzinski, W. E. Biodegradable Polymeric Nanoparticles as Drug Delivery Devices. *J. Controlled Release* **2001**, *70*, 1−20.
(20) Lasprilla, A. J. R.; Martinez, G. A. R.; Lunelli, B. H.; Jardini, A. L.; Maciel Filho, R. Poly-Lactic Acid Synthesis for Application in Biomedical Devices—A Review. *Biotechnol. Adv.* **2012**, *30*, 321−328.
(21) Zhao, Z.; Wang, J.; Mao, H. Q.; Leong, K. W. Polyphosphoesters in Drug and Gene Delivery. *Adv. Drug Delivery Rev.* **2003**, *55*, 483−499.
(22) Wang, Y. C.; Tang, L. Y.; Sun, T. M.; Li, C. H.; Xiong, M. H.; Wang, J. Self-Assembled Micelles of Biodegradable Triblock Copolymers Based on Poly(Ethyl Ethylene Phosphate) and Poly-(Epsilon-Caprolactone) as Drug Carriers. *Biomacromolecules* **2008**, *9*, 388−395.
(23) Xiong, M. H.; Bao, Y.; Yang, X. Z.; Wang, Y. C.; Sun, B.; Wang, J. Lipase-Sensitive Polymeric Triple-Layered Nanogel for "On-Demand" Drug Delivery. *J. Am. Chem. Soc.* **2012**, *134*, 4355−4362.
(24) Mao, C. Q.; Du, J. Z.; Sun, T. M.; Yao, Y. D.; Zhang, P. Z.; Song, E. W.; Wang, J. A Biodegradable Amphiphilic and Cationic Triblock Copolymer for the Delivery of siRNA Targeting the Acid Ceramidase Gene for Cancer Therapy. *Biomaterials* **2011**, *32*, 3124−3133.
(25) Du, J. Z.; Du, X. J.; Mao, C. Q.; Wang, J. Tailor-Made Dual pH-Sensitive Polymer-Doxorubicin Nanoparticles for Efficient Anticancer Drug Delivery. *J. Am. Chem. Soc.* **2011**, *133*, 17560−17563.
(26) Zhang, S.; Zou, J.; Zhang, F.; Elsabahy, M.; Felder, S. E.; Zhu, J.; Pochan, D. J.; Wooley, K. L. Rapid and Versatile Construction of Diverse and Functional Nanostructures Derived from a Polyphosphoester-Based Biomimetic Block Copolymer System. *J. Am. Chem. Soc.* **2012**, *134*, 18467−18474.
(27) Zhang, S.; Zou, J.; Elsabahy, M.; Karwa, A.; Li, A.; Moore, D. A.; Dorshow, R. B.; Wooley, K. L. Poly(Ethylene Oxide)-Block-Polyphosphester-Based Paclitaxel Conjugates as a Platform for Ultra-High Paclitaxel-Loaded Multifunctional Nanoparticles. *Chem. Sci.* **2013**, *4*, 2122−2126.
(28) Li, Q.; Wang, J.; Shahani, S.; Sun, D. D. N.; Sharma, B.; Elisseeff, J. H.; Leong, K. W. Biodegradable and Photocrosslinkable Polyphosphoester Hydrogel. *Biomaterials* **2006**, *27*, 1027−1034.
(29) Li, Y.; Wang, F.; Sun, T.; Du, J.; Yang, X.; Wang, J. Surface-Modulated and Thermoresponsive Polyphosphoester Nanoparticles for Enhanced Intracellular Drug Delivery. *Sci. China: Chem.* **2014**, *57*, 579−585.
(30) Zou, J.; Zhang, F.; Zhang, S.; Pollack, S. F.; Elsabahy, M.; Fan, J.; Wooley, K. L. Poly(Ethylene Oxide)-block-Polyphosphoester-graft-Paclitaxel Conjugates with Acid-Labile Linkages as a pH-Sensitive and Functional Nanoscopic Platform for Paclitaxel Delivery. *Adv. Healthcare Mater.* **2014**, *3*, 441−448.
(31) Sun, C. Y.; Dou, S.; Du, J. Z.; Yang, X. Z.; Li, Y. P.; Wang, J. Doxorubicin Conjugate of Poly(Ethylene Glycol)-Block Polyphosphoester for Cancer Therapy. *Adv. Healthcare Mater.* **2014**, *3*, 261−272.
(32) Molina, I.; Li, S. M.; Martinez, M. B.; Vert, M. Protein Release from Physically Crosslinked Hydrogels of the PLA/PEO/PLA Triblock Copolymer-Type. *Biomaterials* **2001**, *22*, 363−369.
(33) Wang, F.; Wang, Y. C.; Dou, S.; Xiong, M. H.; Sun, T. M.; Wang, J. Doxorubicin-Tethered Responsive Gold Nanoparticles Facilitate Intracellular Drug Delivery for Overcoming Multidrug Resistance in Cancer Cells. *ACS Nano* **2011**, *5*, 3679−3692.
(34) Xiong, M. H.; Wu, J.; Wang, Y. C.; Li, L. S.; Liu, X. B.; Zhang, G. Z.; Yan, L. F.; Wang, J. Synthesis of PEG-Armed and Polyphosphoester Core-Cross-Linked Nanogel by One-Step Ring-Opening Polymerization. *Macromolecules* **2009**, *42*, 893−896.
(35) Yang, X. Z.; Dou, S.; Wang, Y. C.; Long, H. Y.; Xiong, M. H.; Mao, C. Q.; Yao, Y. D.; Wang, J. Single-Step Assembly of Cationic Lipid-Polymer Hybrid Nanoparticles for Systemic Delivery of siRNA. *ACS Nano* **2012**, *6*, 4955−4965.
(36) Yang, X. Z.; Dou, S.; Sun, T. M.; Mao, C. Q.; Wang, H. X.; Wang, J. Systemic Delivery of siRNA with Cationic Lipid Assisted PEG-PLA Nanoparticles for Cancer Therapy. *J. Controlled Release* **2011**, *156*, 203−211.
(37) Zhang, S.; Li, A.; Zou, J.; Lin, L. Y.; Wooley, K. L. Facile Synthesis of Clickable, Water-Soluble, and Degradable Polyphosphoesters. *ACS Macro Lett.* **2012**, *1*, 328−333.
(38) Li, F.; Li, S.; El Ghzaoui, A.; Nouailhas, H.; Zhuo, R. Synthesis and Gelation Properties of PEG-PLA-PEG Triblock Copolymers Obtained by Coupling Monohydroxylated PEG-PLA with Adipoyl Chloride. *Langmuir* **2007**, *23*, 2778−2783.